Investigations of the factors causing performance losses of lead/acid traction batteries

H. Kronberger, Ch. Fabjan and N. Gofas
Institut für Technische Elektrochemie, Technische Universität Wien, Getreidemarkt 9/158, 1060 Vienna (Austria)

(Received October 12, 1993; in revised form December 18, 1993; accepted December 18, 1993)

Abstract

A failure analysis is carried out with a lead/acid traction battery after a two-years' test run in an electric passenger car. A survey of the operational data, in combination with laboratory tests and chemical and physical analyses, reveals the main causes of battery damage and performance loss: insufficiencies of the charging procedure, inadequate maintainance (water-refilling system), antimony-contamination and loss of active material due to grid corrosion and shedding of PbO_2.

Introduction

Lead/acid traction batteries frequently show a significant performance loss in an electric vehicle after a relatively short period of operation. A critical review of the recorded operational data, associated with specific electrochemical laboratory experiments and supported by chemical and physical analyses, should provide a better insight into the complex processes of degradation and reveal the main causes of battery failure.

Experimental

Battery test operation

A lead/acid traction battery was operated, during a two-years' field test, in an electric passenger car (Fiat Panda E) with 990 kp unloaded weight including the battery unit. A d.c. series wound motor with a nominal power of 9.2 kW served as propulsion system.

The users had no specific experience in battery operation.

The main operational data — operation time, charged capacity, mileage, current and voltage at the end of the charge cycle, and additional information about stand-by periods, maintainance or repair activities — were recorded by the respective user.

Figure 1 gives a general view on the operation and stand-by periods.

The battery consisted of 12 units of a clad-type lead/acid system with a nominal capacity of 175 Ah (*C*/5 discharge rate) and a voltage of 6 V per unit connected in series. The cell compartments were equipped with float valves and a semi-automatical water-refilling device using a bypasss system which consisted of two independent loops of flexible tubes. The schematic cell design is given in Fig. 2. Cathodic and anodic

SSDI 0378-7753(93)01894-N

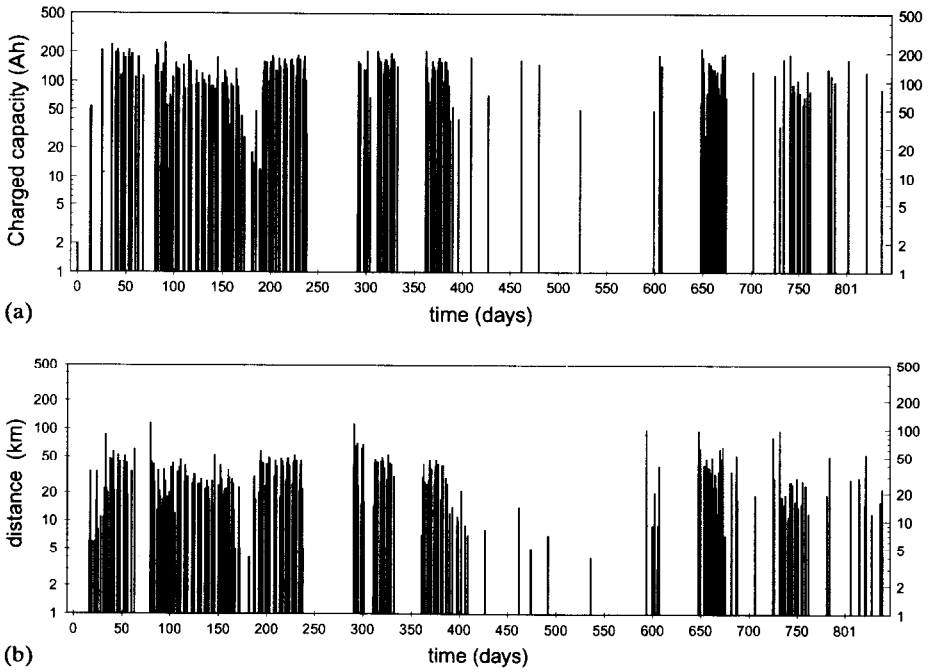

Fig. 1. Battery operation and stand-by periods.

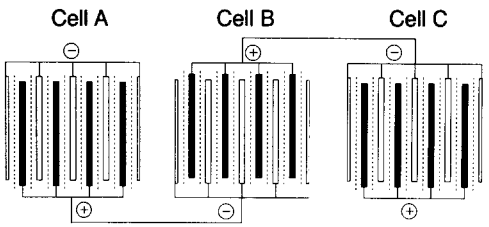

Fig. 2. Schematic cell design.

plates were mounted in a usual monopolar arrangement with single-sided negative terminal plates each containing only 50% of the normal electrode capacity.

During the test period, the battery was recharged in a constant power (W_a) mode by a microprocessor-controlled charging station [1]. After a constant charge current had been established for 20 min, indicating a 100% state-of-charge, the charge process was stopped:

$$\frac{dW_a}{dt} = \frac{d(UI)}{dt} = 0 \tag{1}$$

$$U_{gas} = \text{constant} \longrightarrow \frac{dI}{dt} = 0 \tag{2}$$

Automatical recharge for 17 min every 9 h ensured a full state-of-charge (SOC) of the battery during the stand-by periods.

Laboratory experiments

The single 6-V units were submitted to the following test procedures:

- determination of capacity by constant-current discharge
- internal resistance measurements at various SOCs
- examination of essential battery components by scanning electron microscopy (SEM) and energy disperse system (EDS) surface analysis
- chemical analyses of the electrolyte and the deposited fractions of the active material

Results and discussion

The data show a substantial loss of capacity (Ah) and an increase in specific energy consumption (SEC) (Wh t^{-1} km^{-1}) within two months of operation (Fig. 3).

Several variations in SEC reflect the influence of self-discharge compensated by repeated intermediate charging showing high values of SEC at a low ratio of operation to stand-by periods (Fig. 4).

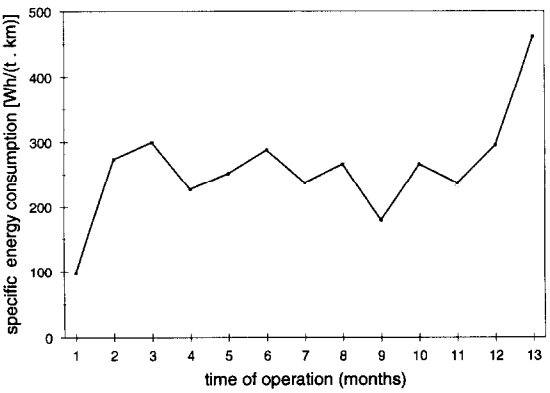

Fig. 3. Mean values of specific energy consumption vs. time of operation.

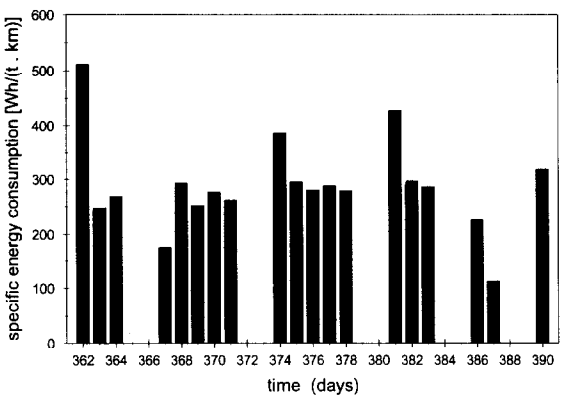

Fig. 4. Specific energy consumption at intermittant operation.

Over the period of operation a steady increase in the current values, marking the end of the constant power charge cycle, corresponds to a voltage decrease at this point.

This phenomenon is apparently caused by a contamination of the lead electrode with catalytically active materials such as antimony, increasing the rate of hydrogen evolution [2, 3].

An extended form of the Arrhenius's equation shows the dependence of the cathodic current density $i_D(\phi)$ (A $cm^{-1})^2$ at a potential ϕ on the Gibbs free enthalpy of activation, ΔG^0_{act}:

$$i_D^-(\phi_2) = -nFc_{ox}k_0' \exp\left[-\frac{\Delta G_{act}(\phi_1) + (1-\alpha)nF\Delta\phi}{RT}\right] \quad (3)$$

$(\Delta\phi = \phi_1 - \phi_2;\ \phi_2 < \phi_1)$

Hence, a decrease in the activation enthalpy should produce an increase in the current density of the electrode reaction considered (hydrogen evolution).

After 21 months of testing, the battery showed poor performance due to losses of capacity and power accompanied by sulfation and increased internal resistance.

Laboratory battery tests

The single 6-V units of the disassembled battery were submitted to a two-step charge process at a constant current (32 A) with a cutoff voltage of 7.2 V. In order to achieve a high charging level (SOC → 100%), the charge process was subsequently continued at 2 A until the same terminal voltage was re-established.

Table 1 shows the efficiencies and the discharge capacities of the single units after several (3 to 5) cycles. A constant discharge current of 32 A has been applied until a voltage of 5.1 V was reached.

The values of coulombic, voltaic and energy efficiencies have been calculated from the voltage–time plots of the corresponding charge/discharge cycles (Fig. 5).

TABLE 1

Discharge capacities and efficiencies

Unit no.	Capacity (Ah)	Efficiency (%)		
		Coulombic	Voltaic	Energy
1	51.7	88.9	84	74.6
2	130.1	97.95	87.5	85.7
3	64	85.1	84.3	71.7
4	46.9	80.7	84.1	67.9
5	47.4	82.4	84.1	69.3
6	78.4	87.5	84.5	73.9
7	46.6	90.6	83.8	75.9
8	65.6	77.3	84.4	65.3
9	118.4	99.1	87.5	86.6
10	97	98.2	87.4	85.5
11	74.1	86.3	83.5	72
12	76.2	84.6	84.4	71.8

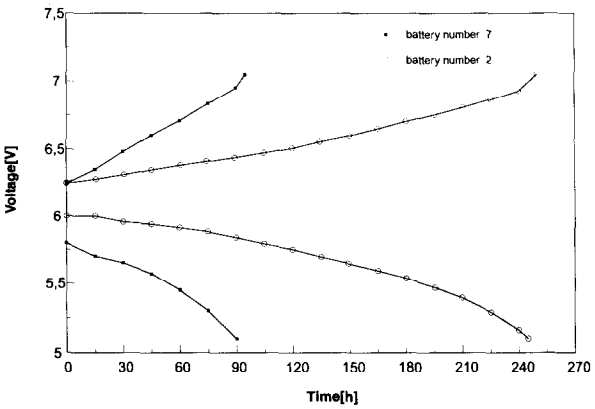

Fig. 5. Charge/discharge cycles.

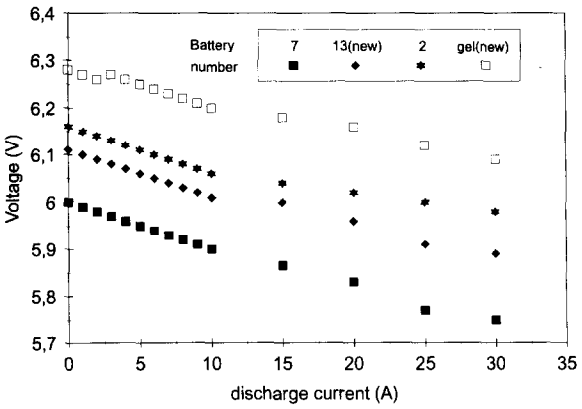

Fig. 6. Current–voltage characteristics.

Steady-state current–voltage characteristics were determined at various SOCs in order to characterize the specific behaviour and the condition of the different units. The ohmic resistance has been calculated from the slope of current–voltage lines which also enable the estimation of the influence of polarization effects on high current densities. The most important results of these measurements are presented in Fig. 6.

The acid concentration was determined by volumetric analysis of electrolyte samples taken from each individual cell compartment at 100% SOC. The expected close correlation between the acid concentration and the discharge capacity due to sulfation could not be found in all cases (Fig. 7).

This result provides strong evidence, that sulfation is not the only process responsible for the loss of sulfuric acid. Changes in the sulfuric acid concentration may also be caused by a loss of non-sulfated active material or simply by dilution of the electrolyte as a consequence of an insufficient operation of the water-refilling system, or by maintainance faults, respectively.

Current–voltage characteristics measured at 10, 50 and 80% SOC show, in general, an ohmic behaviour giving evidence of additional polarization at high current densities.

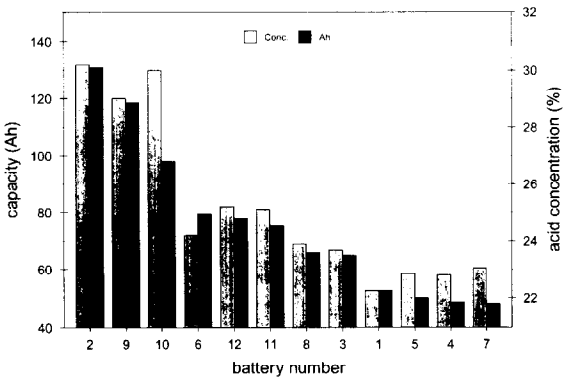

Fig. 7. Discharge capacity and acid concentration (100% SOC).

TABLE 2

Resistance of selected battery units at 25 °C

State-of-charge (%)	Charge resistance (mΩ)				Discharge resistance (mΩ)			
Unit no.	2	7	14	13	2	7	14	13
80	10	11	8	10	10	11	10	10
50	10	11.5	8	10	10	12	10	10
10	12	15	10	10	12	18	10	15

Table 2 lists the resistance of selected 6-V units calculated from the current–voltage plots at different SOCs:

$$\frac{\Delta U}{\Delta I} = R \tag{4}$$

Assuming a pure ohmic behaviour $dR_i/di = 0$, the voltage at the maximum power (U_{max}) can be calculated:

$$U_o = iR_i + iR_a \tag{5}$$

$$U_l = iR_a = U_o - iR_i \tag{6}$$

$$U_l = xU_o \tag{7}$$

$$P(x) = U_l i = xU_o i = x(1-x)\frac{U_o^2}{R_i} \tag{8}$$

$$\frac{dP}{dx} = 0 \longrightarrow x = 0.5;\ iR_i = iR_a = 0.5U_o$$

$$U_{Pmax} = 0.5U_o \tag{9}$$

A comparison between the P_{max} values of unit nos. 2 and 7 and a battery of the same type no. 13 and a maintainance-free battery no. 14, freshly manufactured, provides the additional evidence for the poor condition of unit no. 7.

TABLE 3

P_{max} values of selected units at different states-of-charge (25 °C)

Unit no.	P_{max} (W)			
	2	7	14 (gel)	13 (new)
SOC 80%	917.8	847	1341.8	1033.6
SOC 50%	919.3	712.9	1178.1	1038.5
SOC 10%	632.3	506.7	906.5	630.9

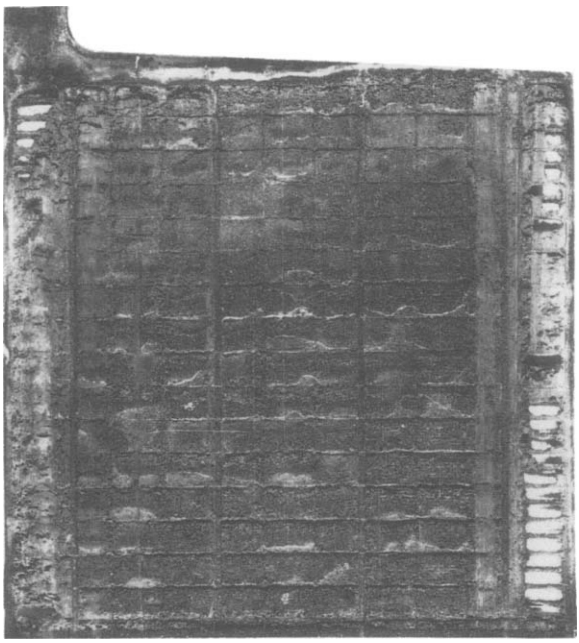

Fig. 8. Grid corrosion.

Disassembling of a unit and component analysis

In order to identify the processes, mainly responsible for the battery's performance losses, unit no. 7 was disassembled to examine the cell components.

Mechanical defects and signs of corrosion were detected in different areas of the negative electrodes. Extensive corrosion was observed preferably at the edges of the negative electrode grid. In addition to the active material layer, the supporting antimony-containing grid had been also exposed to the corrosive attack (Fig. 8).

SEM analysis in general showed a crystalline surface structure with large crystals of pure $PbSO_4$. EDS analysis revealed relatively high amounts of antimony (Fig. 9) due to the corrosion of the antimony-containing supporting material [4].

Sediment analysis

Substantial amounts of the shedded active material (200–300 g) were deposited as a sediment covering the bottom of the single-cell compartments. After separation

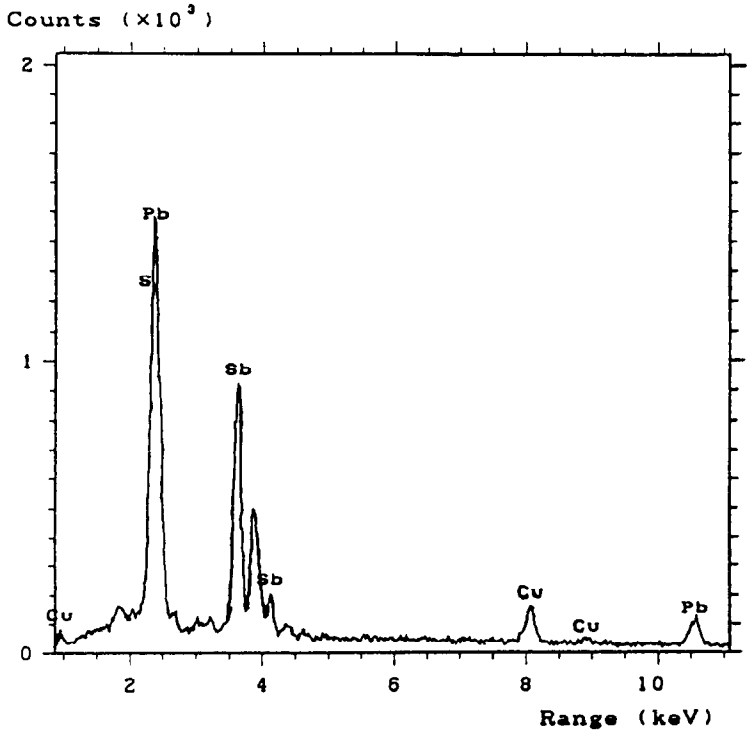

Fig. 9. Surface analysis.

TABLE 4

Sediment analysis

Cell	A	B	C
Total sediment (g)	304.81	236.67	276.16
$PbSO_4$ (wt.%)	24.3	21.9	26.8
PbO_2 (wt.%)	41.26	48.1	39.5
Pb (wt.%)	17.1	19.6	27.6
Humidity (wt.%)	7.34	10.4	6.1
Total (%)	100	100	100

from the electrolyte, the residue was vacuum dried at low temperatures — to avoid decomposition of PbO_2 — with a remaining humidity of approximately 10% w/w.

$PbSO_4$ was separated by dissolution in aqueous ammonium tartrate. The main part of the residue (Pb and PbO_2) was then treated with diluted HNO_3, the residual PbO_2 (IV) reduced by addition of H_2O_2 and the concentration of the resulting Pb^{2+} ions was determined by complexometric titration. The results of the sediment analysis are listed in Table 4.

Several definite findings can be obtained from the results of the failure analysis.

1. A doubling of the specific energy consumption and a significant decrease in capacity occurred within the first two months of the operation of the battery. Despite

these findings, an essential part of the units (about 50%) has kept a rather good performance after two years of operation. This indicates that, in general, the damages are not caused by a frequent deep discharge. This interpretation is also confirmed by the recorded operational data. The batteries evidently recover during stand-by periods due to the application of an intermediate recharge which re-establishes the normal capacity and improves the performance. These effects are enhanced by an additional equalizing charge and an adjusting of the required acid concentration in the single-cell compartments. Significant deviations of the acid concentration at 100% SOC from the expected values are mainly due to an insufficient water-refilling process. For instance, an overflow of single cells can occur if a level-control valve is blocked. The subsequent dilution of the sulfuric acid electrolyte is more deleterious if it occurs incidentally at high SOCs. These assumptions have been confirmed by control tests of the water-refilling system.

2. An early performance loss also indicates a sulfation process due to insufficiencies of the charging system, interrupting the charge process before the battery reaches a 100% SOC. In addition to that, the lack of a periodic equalizing charge supports the variation of the actual SOC of the single cells. SOC differences of the series-connected cells are enhanced with an increasing number of cycles and may cause cell reversal in a deep-discharge process [5].

3. Substantial losses of the active material forming layers of sludge at the bottom of the single-cell compartments — due to a shedding process at the positive plates and a corrosive attack at the negative electrodes — are responsible for the irreversible deterioration of the cell performance and capacity, respectively. The construction of the — thin — negative terminal plates is definitely a weak point, since massive corrosive attack has been observed at these electrodes (Fig. 8). Moreover, the damages observed at the negative electrodes may be the result of a too high acid concentration, occasional charging under short-circuit conditions, or continuous charging at an excessive rate at high temperatures [5]. Future progress can be expected from developments concerning electrolyte management: an improvement of the water-refilling system or the use of maintainance-free batteries, respectively [6–8]. Optimization of the charge process and advanced electrode construction should improve the performance and cycle life of the batteries, and reduce the detrimental effects of sulfation, grid corrosion and antimony poisoning.

List of symbols

α	transfer coefficient
$C/5$	discharge rate (5-h discharge)
c_{ox}	concentration of the oxidized species
EDS	energy disperse system
ϕ	potential
F	Faraday constant
ΔG^0_{act}	Gibbs free enthalpy of activation
I, i	current
i_D^-	cathodic current density
k_0'	rate constant
n	number of electrons per formula unit
p_{max}	maximum power

$\phi_{1,2}$	potential 1, potential 2
R	resistance
R_i, R_a	internal, external resistance
SEC	specific energy consumption
SOC	state(s)-of-charge
t	time
U	voltage
U_o	open-circuit voltage
U_{gas}	gas-evolution voltage
U_l	cell voltage during load
W_a	charging power

References

1 T.R. Crompton, *Battery Reference Book,* Butterworths, London, 1990, Ch. 48.
2 W. Herrmann, *Elektrotech. Z., Ausg. B, 16* (1964) 643.
3 E. Witte, *Blei- und Stahlakkumulatoren,* VARTA Fachbuchreihe, VDI, Düsseldorf, 1977.
4 K. Wiesener, J. Garche and W. Schneider, *Elektrochemische Stromquellen,* Akademie Verlag, Berlin, 1981.
5 K.V. Kordesch, *Batteries,* Vol. 2, Marcel Dekker, New York, 1977.
6 D. Pavlov, in B.D. McNicol and D.A.J. Rand (eds.), *Power Sources of Electric Vehicles,* Elsevier, Amsterdam, 1984.
7 J. Brinkmann, *Oesterr. Z. Elektrizitätswirtsch., 46* (1993) 477.
8 H. Tuphorn, *J. Power Sources, 40* (1992) 47–61.